RESEARCH ARTICLE
SOLID EARTH: GEODYNAMICS

Earth and Planetary Physics
2: 52–66, 2018
doi: 10.26464/epp2018005

Thermal structures of the Pacific lithosphere from magnetic anomaly inversion

Chun-Feng Li[1,2*], and Jian Wang[3]

[1]Department of Marine Sciences, Zhejiang University, Zhoushan 316021, China;

[2]Laboratory for Marine Mineral Resources, Qingdao National Laboratory for Marine Science and Technology, Qingdao 266237, China;

[3]Key Laboratory of Crustal Dynamics, Institute of Crustal Dynamics, Chinese Earthquake Administration, Beijing 100085, China

Abstract: Of the world's oceans, the Pacific has the most abundant distribution of seamount trails, oceanic plateaus and hot spots, and has the longest fracture zones. However, little is known of their thermal structures due to difficulties of heat flow measurement and interpretation, and in inferring thermal anomalies from low-resolution seismic velocities. Using recently published global magnetic models, we present the first independent constraint on Pacific geothermal state and mantle dynamics, by applying a fractal magnetization inversion model to magnetic anomaly data. Warm thermal anomalies are inferred for all known active hot spots, most seamount trails, some major fracture zones, and oceanic lithosphere between ~100 and ~140 Ma in age. While most Curie points are among the shallowest in the zone roughly bounded by the 20 Ma isochrons, abnormally deep Curie points are found along nearly all ridge crests in the Pacific, related to patchy, long-wavelength and large-amplitude magnetic anomalies that are most likely caused by prevailing magmatic or hydrothermal processes. Many large contrasts in the thermal evolution between the Pacific and North Atlantic support much stronger hydrothermal circulation occurring in Pacific lithospheres younger than ~60 Ma, which may have disguised from surface heat flow any deep thermal signatures of volcanic structures. Yet, at depths of the Curie points, our model argues for warmer Pacific lithosphere for crustal ages older than ~15 Ma, given a slightly higher spatial correlation of magnetization in the Pacific than in the North Atlantic.

Keywords: Pacific; Curie depth; heat flow; seamount; oceanic plateau; magnetic anomaly

Citation: Li, C.-F., and Wang, J. (2018). Thermal structures of the Pacific lithosphere from magnetic anomaly inversion. *Earth Planet. Phys.*, *2*, 52–66. http://doi.org/10.26464/epp2018005

1. Introduction

The lithosphere of Pacific basin currently comprises, entirely or partially, several tectonic plates, i.e. the Pacific, Nazca, Antarctic, Cocos, and Juan de Fuca plates, which are divided by active spreading centers (Figure 1). Relict spreading centers have been identified in the two largest plates, the Pacific and Nazca plates (e.g., Taylor, 2006; Müller et al., 2008), suggesting a complicated multi-phased evolutional history. One of the most striking and enigmatic features in the Pacific is its widespread seamount chains, which are often subparallel to seafloor spreading directions (Figure 1). There are also numerous large igneous plateaus, such as the Ontong Java, Manihiki and Hikurangi Plateaus, that are often associated with changes in seafloor spreading regimes. Various mechanisms have been hypothesized to explain these igneous features, including mantle plumes and superplumes (Morgan, 1972; Davaille, 1999), small scale convection (Bonatti and Harrison, 1976; King and Ritsema, 2000; Ballmer et al., 2010), regional extension in various forms of thermomechanical fracturing and cracking (Collette, 1974; Turcotte, 1974; Gomez and Briais, 2000; Sandwell and Fialko, 2004), diffuse extension (Sandwell et al., 1995; Davis et al., 2002; Stepashko, 2006), and transform fault rupturing (Orwig and Kroenke, 1980; Farrar and Dixon, 1981). Study of deep thermal structures can help better understand these seamount volcanisms.

Global bathymetric surveys show that, among the global oceans, the Pacific has the most abundant seamounts taller than 3 km (Kim and Wessel, 2011), and extant oceanic plateaus occur mostly in the Pacific (Kerr and Mahoney, 2007). One way to better understand their geodynamic origins is to determine the deep thermal structures of these igneous features, along with the cooling of surrounding oceanic lithosphere. We gridded a total of 31032 heat flow measurements from the Global Heat Flow Database of the International Heat Flow Commission (http://www.heatflow.und.edu/), last updated in January 2011, to map the near-surface thermal structure of Pacific lithosphere (Figure 2). Without any preprocessing or pre-selection, the heat flow data are gridded with a block mean in a constant 1° interval, using the minimum curvature algorithm with a tension factor of 0.5 (Wessel and Smith, 1995). Averaging of heat flow over a large spatial dimension suppresses local biases in the measurements and generally gives more regional and deeper geothermal information (Mareschal and Jaupart, 2004; Li et al., 2013). Hasterok et al.

Correspondence to: C.-F. Li, cfli@zju.edu.cn
Received 31 AUG 2017; Accepted 15 DEC 2017.
Accepted article online 23 DEC 2017.

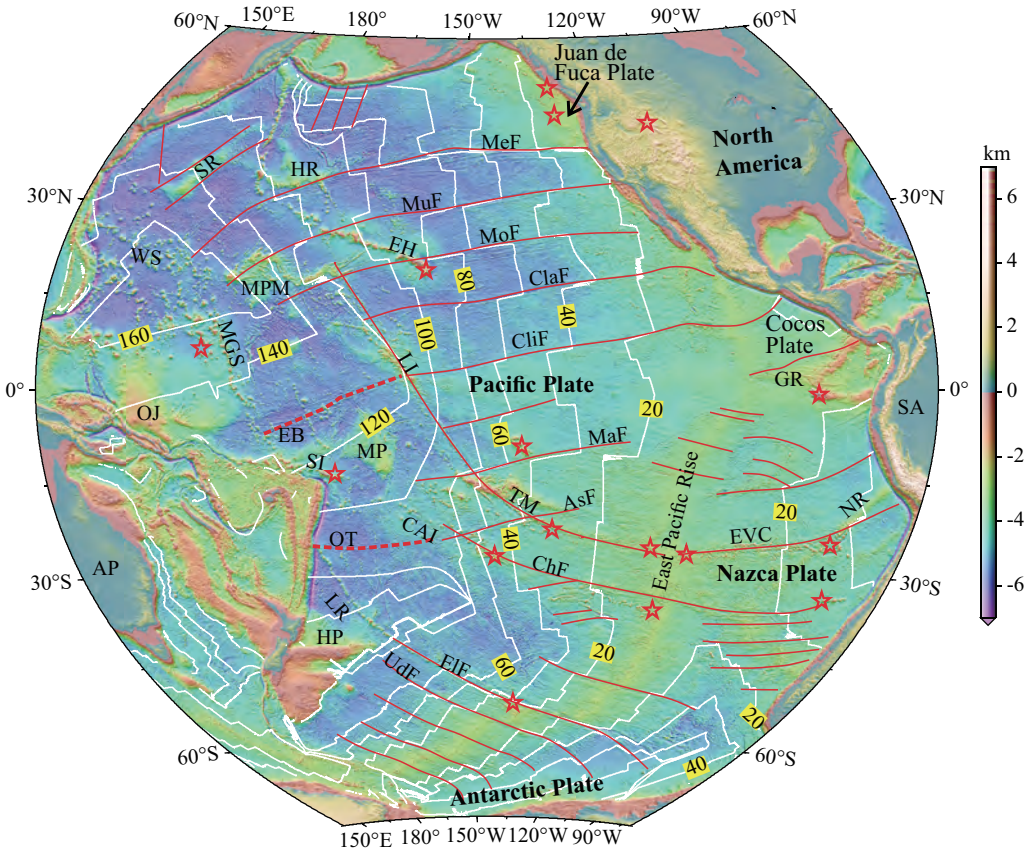

Figure 1. Pacific bathymetry and topography map in Hammer-Aitoff equal-area projection (Data from Smith and Sandwell, 1997). Crustal isochrons in white are based on Müller et al. (2008). Thin red lines are fracture zones. The thick red dashed line labels relict spreading centers. Red stars label major active hot spots. Features marked are Astral Fracture Zone (AsF), Australian Plate (AP), Challenger Fracture Zone (ChF), Clarion Fracture Zone (ClaF), Clipperton Fracture Zone (CliF), Cook-Australs Islands (CAI), Ellice Basin (EB), Eltanin Fracture Zone (ElF), Emperor-Hawaii seamount chain (EH), Easter Volcanic Chain (EVC), Galapagos Ridge (GR), Hess Rise (HR), Hikurangi Plateau (HP), Line Islands (LI), Louisville Ridge (LR), Manihiki Plateau (MP), Marquesas Fracture Zone (MaF), Marshall Gilbert Seamounts (MGS), Mendocino Fracture Zone (MeF), Mid-Pacific Mountains (MPM), Molokai Fracture Zone (MoF), Murray Fracture Zone (MuF), Nazca Ridge (NR), Ontong-Java Plateau (OJ), Osbourn Trough (OT), South America (SA), Samoa Islands (SI), Shatsky Rise (SR), Taumotu Islands (TM), Udintsev Fracture Zone (UdF), and Wake Seamounts (WS).

(Hasterok et al., 2011; Hasterok, 2013) filtered heat flow data by sediment thickness and distances to seamounts, to remove hydrothermal effects on background conductive heat flow. We believe that large-dimension interpolation can achieve similar goals of removing local biases from hydrothermal effects without any specific filtering.

In making the heat flow map (Figure 2), we have masked areas that are over 500 km away from any nearby heat flow points. Nevertheless, no direct correlation between surface heat flow and seamounts/plateaus is observed from comparing Figures 1 and 2, consistent with previous observations on the south Pacific superswell (Stein and Abbott, 1991), Iceland (Stein and Stein, 2003), and Hawaiian Islands (Von Herzen et al., 1989; McNutt, 2002; Stein and Von Herzen, 2007). High heat flow anomalies in the Pacific are mostly associated with active spreading centers.

The questions now are how well the interpolated heat flow reflects deep geothermal structure, or, in other words, whether we have an alternate mechanism for detecting high-resolution lithospheric thermal structure that might differ sharply from what we can perceive from the surface heat flow.

In recent years, we have demonstrated a stable automated algorithm for estimating Curie-point depths at a relatively high resolution, and successfully applied it to oceanic domains such as the North Atlantic (Li C-F et al., 2013), the South China Sea (Li C-F et al., 2010; Li C-F and Wang, 2016), and the northern Philippine Sea (Li C-F, 2011; Li C-F and Wang, 2016). Here, we estimate the Curie-point depths of the Pacific basin to give a geothermal constraint independent of heat flow. This assumes that there is magnetized material present at depth and possibly at sub-crustal depths, which requires serpentinization of the mantle (e.g. Oufi et al., 2002), in-situ magnetization of the mantle (Arkani-Hamed, 1989) or in the volcanic conduit (Ferré et al., 2013). We can also compare the information gained from Curie depths to the thermal structures, e.g., inferred by Ritzwoller et al. (2004) from seismic velocities of the Pacific lithosphere.

On the cooling process of oceanic lithosphere, many mechanisms have been proposed to explain the apparent flattening of both heat-flow and bathymetry versus age curves of old oceanic lithosphere. These include small-scale convection (Parsons and McKenzie, 1978), radioactive heating (Forsyth, 1977), shear stress heat-

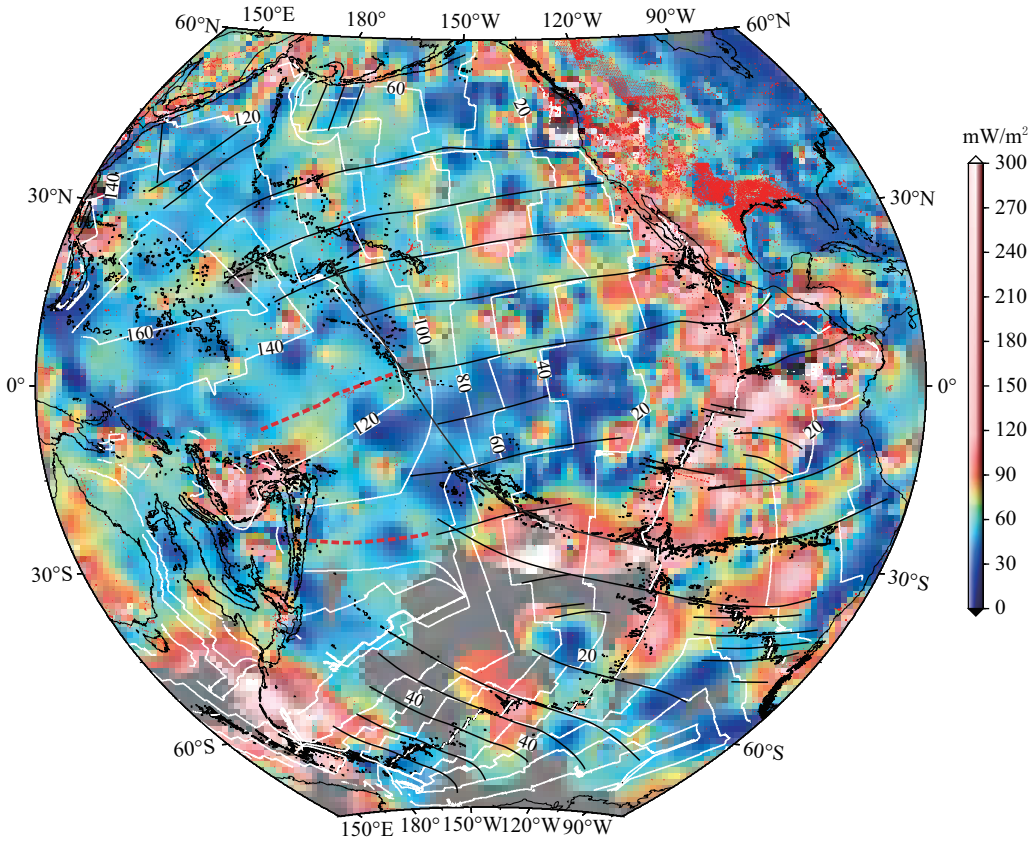

Figure 2. Heat flow map of the Pacific in Hammer-Aitoff equal-area projection. Data points are gridded with a 1° interval. Red dots show the locations of heat flow measurements. Thin black lines are fracture zones, coastlines and isobaths. White lines show isochrones. The thick red dashed line labels relict spreading centers. See Figure 1 for more annotations.

ing (Schubert et al., 1976), asthenospheric flow (Phipps Morgan and Smith, 1992), plumes (Davies, 1988), hotter and thinner lithosphere (Stein and Stein, 1992), and trapped heat (Huang JH and Zhong SJ, 2005). There remain conflicting arguments on whether seafloor flattening could still persist, if (1) hot spots and oceanic plateaus were removed (Schroeder, 1984; Hillier and Watts, 2005; Korenaga and Korenaga, 2008), or if (2) the bathymetry were to be observed along mantle flow lines rather than along trajectories normal to isochrons (Adam and Vidal, 2010). Estimated Curie-point depths, reflecting a deep isotherm, should help answer these questions.

In this study, we start with a brief overview of the evolutionary stages of the Pacific, followed by a summary of our algorithm of Curie depth estimation. We then show our Curie depth model, which provides significant geothermal information not seen from surface heat flow, and interpret our results with a particular focus on seamounts and plateaus. At the end, we compare results from the Pacific and the North Atlantic and demonstrate an apparent large difference in their thermal structure. This paper can be considered as a companion paper of Li C-F et al. (2013), which studied thermal evolution of the North Atlantic based on Curie depths.

2. Geology of the Pacific Ocean

To facilitate subsequent discussions, here we review briefly the geological evolution of the Pacific Ocean basin. The magnetic lineations (Figure 3) and their age progressions (e.g., Müller et al., 2008) reveal the multi-phased evolution of Pacific seafloor spreading, which may have exploited pre-existing transform faults since new phases of opening have often tended to be perpendicular to pre-existing transform faults. The oldest seafloor of ~ 180 Ma is in the western Pacific (Nakanishi et al., 1989; Tominaga et al., 2008). Progressive seafloor spreading in the Ellice Basin (EB) (from ~140 to ~120 Ma) and that along the Osbourn Trough (OT) (from ~120 to ~90 Ma, Downey et al., 2007) opened new oceanic basins. These spreading events and ridge jumps may have separated the largest oceanic plateau, the Ontong Java-Manihiki-Hikurangi Plateau (Billen and Stock, 2000; Taylor, 2006; Hoernle et al., 2010). Around 80 Ma, a large unified spreading ridge formed, and it continued to evolve to be the present-day East Pacific Rise. To the east of the East Pacific Rise, the evolution of oceanic lithosphere is more eventful over the past 80 Ma; a large part of old lithosphere has been subducted beneath the North and South American plates, and several recent and active spreading centers have also developed, with various Euler poles (Figures 1 and 3).

The present Euler pole of spreading along the East Pacific Rise also varies in spreading directions, but can be roughly divided into three groups along the strike, based on the layout of transform faults and magnetic anomalies (Figures 1 and 3). The Pacific-Antarctica spreading center, to the south of the Challenger Fracture Zone (ChF) and the Line-Tuamoyu Islands (LI-TM) (Figure 1), is subparallel to the relict spreading centers of the Osbourn Trough

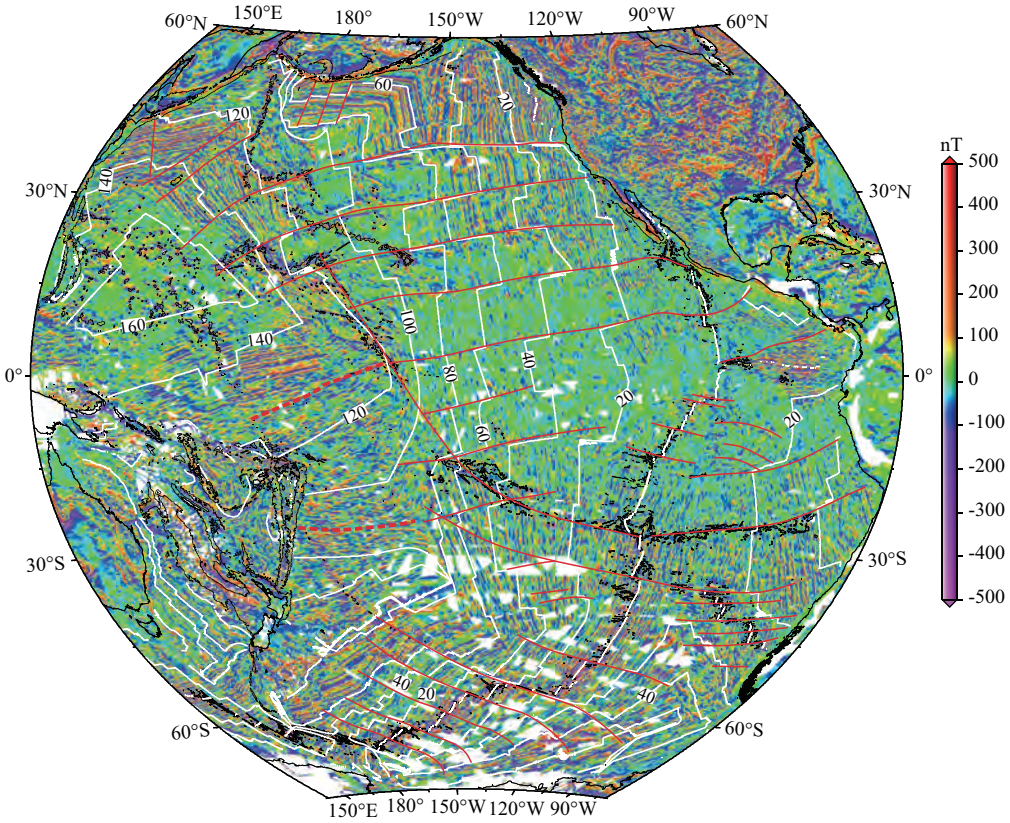

Figure 3. Pacific magnetic anomalies based on EMAG2 (Maus et al., 2009). See Figure 1 for more annotations.

and in the Ellice Basin, and represents the last phase of a series of seafloor spreading events involved with the breakup of Gondwanaland (Hoernle et al., 2010). Transform faults associated with the Pacific-Antarctica spreading center are in a northwest-southeast orientation, contrasting sharply to those large trans-Pacific transform faults to the north, which are almost in an east-west orientation (Figure 1).

The area between the Clipperton Fracture Zone (CliF) and the Line-Tuamotu Islands-Easter Volcanic Chain (LTI-EVC) is transitional, showing both older northwest-southeast trending and younger east-west trending transform faults in the Pacific Plate. Based on the magnetic anomalies and crustal ages, this transition occurred around 20 Ma, almost coeval to the cessation of the Nazca Ridge volcanism and the onset of the Easter volcanism, which are estimated at about 23 Ma (Ray et al., 2012). From the configuration of magnetic anomalies (Figure 3), we did not observe a major change in Pacific plate motion or seafloor spreading configuration around 50 Ma, at the newly proposed timing of initiation of the Hawaii-Emperor bend by Sharp and Clague (2006). It is also worth pointing out that, based on our interpretation of magnetic anomalies and transform faults, the so-called south Pacific superswell (McNutt and Fischer, 1987), a region largely between the Marquesas Fracture Zone (MaF) and ChF, and of abnormally shallow bathymetry and low seismic velocities, is located in the transitional zone of Euler poles; the transform faults that intersect in this region divide into two groups of orientations (Figure 1) reflecting changes in spreading modes. Hillier and Watts (2005) suggest that the superswell is part of a larger, continuous, and monotonic depth-age subsidence trend, but not an isolated shallowing of lithosphere.

Pacific fracture zones may have, in general, remained strong throughout their lifetimes (Kruse et al., 1996). However, many volcanic island chains coincide spatially with large fracture zones or their projected tracks, or with magnetic anomaly boundaries (Figure 1), raising the question whether volcanism might be related to extension and leaking along fracture zones or similarly weak zones (e.g., Sandwell et al., 1995; Smoot and King, 1997; Davis et al., 2002; Koppers et al., 2003; Stepashko, 2006). Among them, the LTI-EVC is the most notable feature that has developed roughly along a long fracture zone that nearly bisects Pacific basin lithosphere.

The seamount ages along Pacific volcanic chains decrease mostly, but not always, toward the spreading center, i.e., becoming younger in the opposite directions to the plate motions (e.g., Koppers et al., 1998, 2001). However, by no means does this observation indicate that these seamounts sourced from relatively fixed mantle plumes; it may simply imply that intraplate volcanisms tend to occur progressively toward younger and thinner oceanic lithosphere. Intraplate seamount and plateau volcanism appear to occur preferably in a certain time window after the lithosphere is formed at the spreading ridge, for example in the Nazca Ridge and the Easter Volcanic Chain (O'Connor et al., 1995; Ray et al., 2012). Sager (1992) estimated from paleomagnetism that there appears to be a significant fraction of seamounts with ages within about 20 Ma of the underlying seafloor of the Pacific Plate. Most active intraplate hot spots, not necessarily fixed (Koppers et al.,

2001), are located either at areas of young oceanic lithosphere or close to large fracture zones.

A second area of dense clustering of seamounts is located in the oldest part of the Pacific Plate (Figure 1), which includes nearly all seamounts older than 70 Ma in the western Pacific (Koppers et al., 2003). In this area are three of the largest oceanic plateaus on the Earth: Shatsky Rise (~140 Ma in age, Mahoney et al., 2005), Ontong Java-Manihiki-Hikurangi (~120 Ma in age, Tarduno et al., 1991; Timm et al., 2011), and Hess Rise (~100 Ma in age, Windom et al., 1981). All three can be classified as on-ridge plateaus, because they formed at or near triple junction mid-ocean ridges (Hilde et al., 1976; Vallier et al., 1981), more or less contemporaneously with underlying and surrounding oceanic lithosphere (Hillier, 2007; Heydolph et al., 2014). Sedimentation records indicate that these plateaus erupted mostly in a submarine environment at various water depths instead of subaerially (Ito and Clift, 1998; Kerr and Mahoney, 2007).

3. Curie Depth Estimation

3.1 Technical Considerations

The technique applied in this study does not assess the depth to the base of the magnetic layer (taken as the Curie depth) directly from the nonlinear inversion, because (1) the deeper Curie depths are revealed more narrowly in very small wavenumber bands, and therefore are more difficult to estimate, and (2) nonlinear direct inversion is prone to being unstable (Li C-F et al., 2010). Instead, we use a linearized least squares inversion in each 2D computational window of magnetic anomalies to capture the depths to the centroid and top of the magnetic layer, at small and large wavenumber bands of radially averaged amplitude (or power) spectra, respectively. Curie depths are then computed algebraically from the centroid and top depths (Tanaka et al., 1999; Li C-F et al., 2009, 2013). The tradeoff of estimating the depth to the centroid and top of the magnetic layer is that shallower interfaces can be better resolved on amplitude spectra and are therefore easier to estimate. Our automated spectral method has been successfully applied in many different places around the world (e.g., Li C-F et al., 2009, 2013), and has proven to be computationally fast and stable, and gives high resolution results.

There are limitations in detecting deep Curie depth targets from geophysical data. The mathematical model we apply is based on infinite horizontal extension (Blakely, 1995), but in reality this is not achievable for real data. Theoretically, magnetic anomalies from deeper sources are more attenuated by the Earth filter, and the result of this is that we have to deal with narrow bands of long wavelengths. These theoretical limitations apply to all Curie depth inversion techniques. In reality we cannot just select the very small wavenumbers that contain centroid depth information, but for computational stability must choose a wider band including some larger wavenumbers. This procedure tends to underestimate the true Curie depths, but this can be circumvented by choosing a smaller fractal exponent β_{3D}^{p} that gives best fitting results to observed geological constraints. A 3D fractal magnetization model has a power spectrum of magnetization proportional to the norm of the wavenumber raised to the power $-\beta_{3D}^{p}$:

$$\phi_{\mathrm{M}}(k_x,k_y,k_z) \propto k^{-\beta_{3D}^{p}},$$

in which $\phi_{\mathrm{M}}(k_x,k_y,k_z)$ is the 3D power spectrum of the magnetization, k_x, k_y, and k_z are wavenumbers in x, y, and z directions respectively, and their Euclidean norm $k = \sqrt{k_x^{\,2}+k_y^{\,2}+k_z^{\,2}}$.

In computing radial amplitude spectra, we apply a constant wavenumber interval of 0.006 km^{-1}. The centroid depths are estimated primarily from the spectral wavenumber range of 0.003–0.03 km^{-1}, and the top depths to the magnetic sources are estimated within the wavenumber range of 0.03–0.08 km^{-1} (Figure 4). These ranges are identical to those we applied in the North Atlantic case (Li C-F et al., 2013). In order to allow regional correlation, relatively fixed wavenumber ranges are preferred over subjective visual selections of wavenumber ranges.

Long-distance spatial correlation of magnetization increases the long wavelength components in the surface magnetic anomalies and will result in large apparent Curie depths. In general, the degree of correlation, quantified by a fractal exponent β_{3D}^{p} defined for the power spectrum of a 3D magnetization (Li C-F et al., 2013), is not known beforehand. Normally a constant fractal exponent is assumed for a particular region, and its value can be constrained to some degree by examining whether the estimated Curie depths are consistent with true geological constraints. For example, at places with active volcanoes, the Curie point depths should be shallow (Li C-F et al. 2009; Li C-F, 2011), and along active spreading centers Curie depths should be close to seafloor

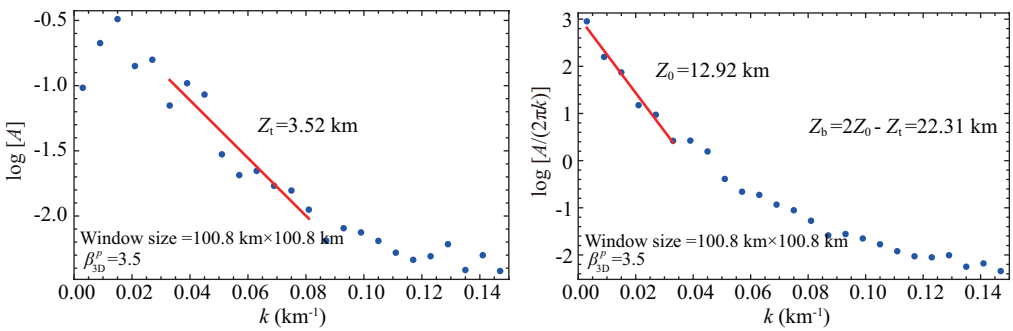

Figure 4. A typical example of (a) amplitude spectrum for estimating depth to the top of magnetic source Z_t, and (b) wavenumber-scaled amplitude spectrum for estimating depth to the centroid of magnetic source Z_0. k, wavenumber; A, amplitude; β_{3D}^{p}, fractal exponent.

depth (Li C-F et al., 2013).

In some previous studies, correlation exponents were estimated from visual picking and varied from window to window (e.g., Bansal et al., 2011). We do not suggest visually picking variable correlation exponents based on the calculated spectra from different windows, because this practice is more subjective and tends to smear out true geological information. True geological constraints on β^p_{3D}, such as from active mid-ocean ridges and volcanoes with better known Curie depths, are always much better than purely mathematical or other technical constraints.

We found from the theories of Blakely (1995) and Maus et al. (1997) that, for β^p_{3D}>0, wavenumber-scaled radially-averaged amplitude spectra of magnetic anomalies always decrease in amplitude monotonically with increasing wavenumber (Li C-F et al., 2013). The theoretical model requires an infinite extension. If the first one or two points in calculated wavenumber-scaled amplitude spectra have smaller in amplitudes at the smallest wavenumbers than the following data points in the spectra (i.e. there are peaks in the spectra), this is likely due to limitations in the calculating window. The best remedy, in our experience, is not to increase the window size, but to judge automatically if there are peaks in the spectra and, if so, to ignore these anomalous points at the smallest wavenumbers, because the theoretical model says that such peaks cannot occur (Li C-F et al., 2013). Alternatively, occurrence of peaks in wavenumber-scaled radially-averaged amplitude spectra can also be used to indicate that we may have overcorrected the spectra with a too large β^p_{3D}.

It should be noted that our algorithm and theory do not consider how the magnetization is captured (Li C-F et al., 2013) and how it evolves with time, whether changing in intensity through low temperature alteration of the ocean crust (Bleil and Peterson, 1983), paleo-intensity variations (e.g., Gee et al., 2000), or potential progressive viscous magnetization of the lower crust and upper mantle (Arkani-Hamed, 1989). For the theoretical background, technical details and caveats of estimating Curie depth from surface magnetic anomalies, the readers are referred to Blakely (1995), Maus et al. (1997), Tanaka et al. (1999), Bouligand et al. (2009), and Li C-F et al. (2013). Although error analysis seems appealing to better quantify errors in the inversion, our judgment is that so many factors can affect the final result that error analysis based on a single or just a few factors, such as errors in the linear regression, would be meaningless.

3.2 Curie Depth Estimation in the Pacific

Our inversion is based on the Earth Magnetic Anomaly Grid of 2-arc-minute resolution (EMAG2, http://geomag.org/) (Figure 3) (Maus et al., 2009), which is compiled from satellite, ship, and airborne magnetic measurements, and is a significant update of a previous 3-minute candidate grid for the World Digital Magnetic Anomaly Map (EMAG3, http://geomag.org/) (Maus et al., 2007).

In EMAG2, the altitude is 4 km above the geoid, with additional grid and track line data included, over both land and the oceans. Directional gridding by least squares collocation using an anisotropic correlation function has been applied to improve the representation of the oceanic magnetic lineations (Maus et al., 2009). This procedure may lead to smoother results than the true magnetic field (Maus et al., 2009), and potentially alter the spectral content of the underlying data and thereby our estimated Curie depths. However, Maus et al., (2009) noted that the anisotropy of the true correlation function was maintained, and the anisotropy of the oceanic field in EMAG2 is realistic. Comparison between EMAG2 and EMAG3 in the North Atlantic has demonstrated that the effect of directional gridding is minimal (Li C-F et al., 2013). In our calculations, we have excluded areas constrained only by satellite data and masked them in the original magnetic maps (Figure 3).

We divide the study area (Figure 1) into 28 zones to facilitate transformation back and forth between spherical and Cartesian coordinates using the ellipsoidal transverse Mercator projection. After estimating Curie depths from these zones we combine them together for final mapping in the Hammer-Aitoff equal-area projection (Figure 5). As we have computed previously for the North Atlantic case (Li C-F et al., 2013), our final Curie depth model (Figure 5) of the Pacific basin is built on an average of Curie depths estimated using two different window sizes, 100.8 km×100.8 km and 201.6 km×201.6 km, and respectively two different moving steps of 50.6 km and 67.2 km. This stacking of results from two different scales helps suppress random noise from using a single window size, and at the same time increases the resolution of the Curie depth model. In this study we computed a total of 151908 points for Curie depths, all with reference to the geoid. This large number of estimates results from using overlapping windows and two different window sizes.

Some previous studies argued that extremely large windows (e.g., ~500 km×500 km) are needed to capture large Curie depths (e.g., Chiozzi et al., 2005; Ravat et al., 2007). By contrast, our previous theoretical and numerical investigations have demonstrated that extremely large windows are not necessary (Li C-F et al., 2010, 2013). It is true that a larger window will give more long-wavelength components and probably increase the stability of the inversion, but since the inversion for the centroid depth is done in the very small wavenumber band, the increased wavelength from using a larger window does not contribute much in the computation, and certainly cannot compensate the loss in resolution due to large window averaging.

For the Pacific basin, we find that a slightly larger fractal exponent β^p_{3D}=3.5 than we applied in the North Atlantic case (Li C-F et al., 2013) and in the global reference model (GCDM; Li C-F et al., 2017), where β^p_{3D}=3.0, is more suitable. This slight change in fractal exponent does not lead to a very different result, but just slightly decreases the average Curie depth. A fundamental difference between the North Atlantic and the Pacific is that the faster spreading Pacific has, in general, wider and thereby more spatially correlated magnetization and magnetic anomalies, warranting the slightly larger β^p_{3D} in the Pacific. The critical reference points for β^p_{3D} are at the mid-ocean ridge, where the estimated depths to both the top and the bottom of the magnetic layer should be close to the water depths of the mid-ocean ridge. This is clearly the case in North Atlantic (Li C-F et al., 2013). However, for the East Pacific Rise, the Curie depths are anomalously large near the ridge crest. This makes it difficult to select the best-fit

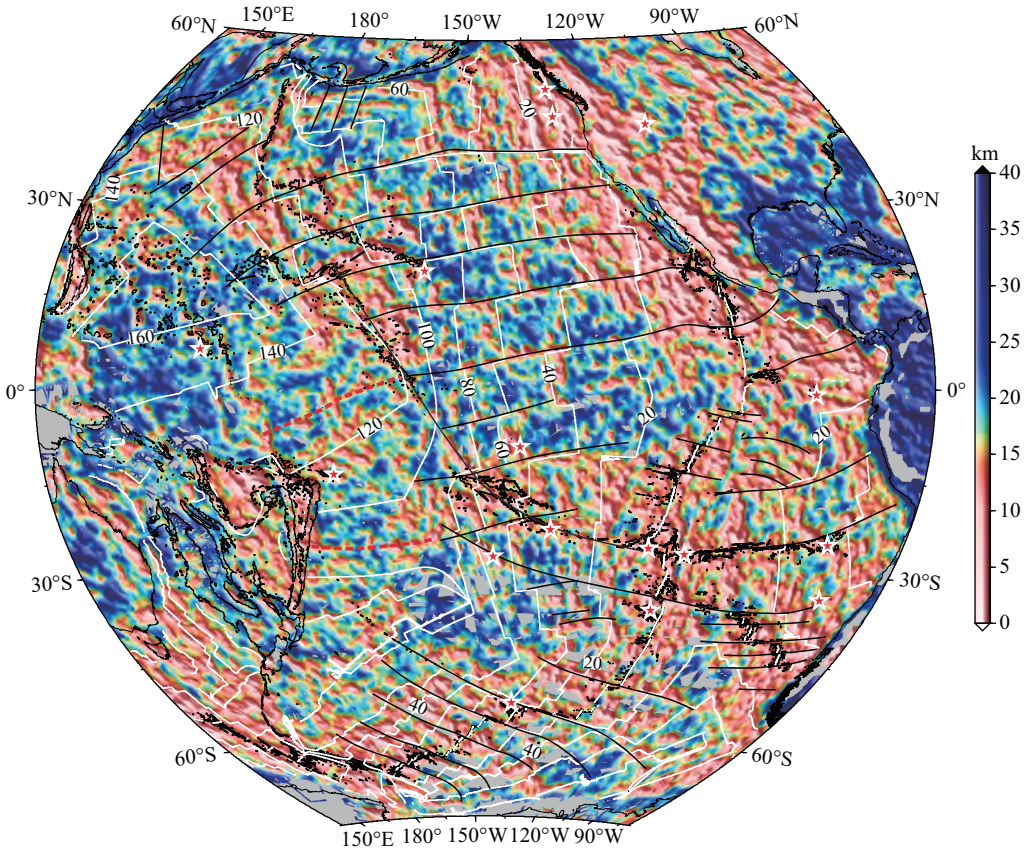

Figure 5. Curie depth map based on magnetic anomalies from EMAG2. The Curie depth model is built on the average of Curie depth estimates from using two different window sizes of 100.8 km×100.8 km and 201.6 km×201.6 km, and a fractal exponent β_{3D}^{p} = 3.5 for the spatial correlation of 3D magnetization. See Figure 1 for more annotations.

β_{3D}^{p}, but a larger β_{3D}^{p} seems to be necessary to place shallower Curie isotherm closer to the ridge crest. We choose this fractal exponent β_{3D}^{p}=3.5 also based on the overall variation of Curie depths with age of the entire Pacific basin.

4. Thermal Structure Inferred from Curie Depth

4.1 Oceanic Lithosphere

Proximal to active spreading centers, Curie depths are evidently among the shallowest in the Pacific (Figure 5). To the east of the East Pacific Rise, Curie depths are relatively small (mostly < 15 km) due to the relatively young oceanic lithosphere and presence of multiple active and relict spreading centers. To the west of the East Pacific Rise, there appears a belt of shallow Curie depths roughly along the Line-Taumotu Island Chain and its northwestern extension into the area proximal to the Emperor-Hawaii seamount chain (EH) (Figure 5). Like the Line-Taumotu Island Chain itself, this belt of shallow Curie depths also appears to bisect the Pacific Plate, with larger Curie depths to either side. The crustal ages covered by this belt range mostly from 100 to 140 Ma in the northwest, and this belt intercepts isochrons from 100 to 0 Ma in the southeast, in the area known as the south Pacific superswell.

Assuming that there is a magnetic phase in the oceanic mantle (e.g., Oufi et al., 2002; Ferré et al., 2013), which has already been suggested and observed in the North Atlantic (Li C-F et al., 2013), the South China Sea (Li C-F et al., 2010), and the northern Philippine Sea (Li C-F, 2011), the Curie depths points assume the Curie temperatures (~550 °C) at the bottom of the magnetic layer. We find that the thermal evolution of the Pacific lithosphere does not strictly follow theoretical expectations (e.g., half-space cooling, Carlson and Johnson, 1994), but shows thermally anomalous regions that are not apparent from surface heat flows (Figure 2). High surface heat flow correlates well with small Curie depths near the active spreading centers, where the lithosphere is thin. Away from the ridges, surface heat flows do not show the anomalous Curie depth features. Surface heat flow measurements are more sensitive to shallow hydrothermal perturbations and sediment variations, whereas Curie depths are more indicative of deep lithospheric thermal structures.

To better understand the thermal evolution of the Pacific lithosphere, we plot Curie depth variation with crustal age (Figure 6). While Curie depths increase with crustal age to the first order, there is a large bump in Curie depths between ~100 and ~140 Ma, also evident in the map (Figure 5). Furthermore, these data do not fit the reference theoretical half-space cooling curve of the 550 °C isotherm, which best fits the North Atlantic Curie depths for crust younger than 40 Ma; for ages less than 15 Ma, the estimated Curie depths are deeper than the theoretical curve, whereas for older ages Curie points are located above the theoretical curve. Equival-

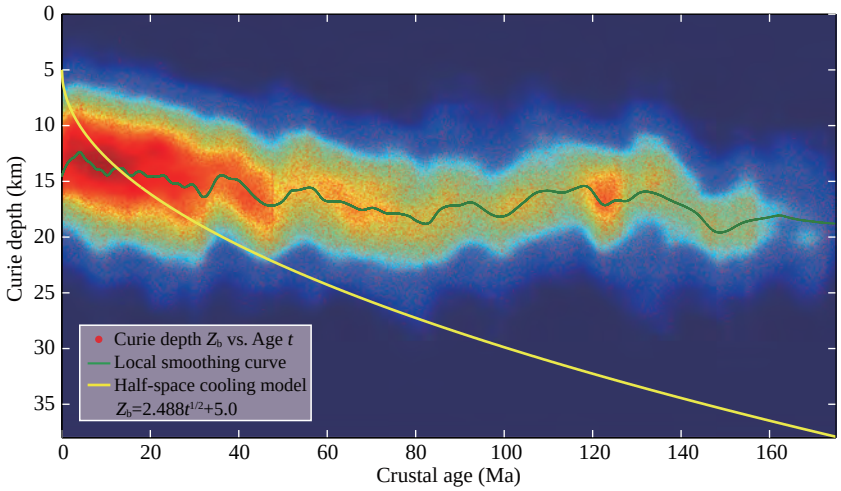

Figure 6. Pacific Curie depth (Z_b) variation with crustal ages (t). Red dots are original estimates of Curie points. Density plot of data are also shown in the background. Green trend is from locally weighted scatterplot smooth using linear least squares fitting and a second-degree polynomial.

ently, younger Pacific lithosphere near the active spreading centers appears to be cooler, whereas older lithosphere appears to be much warmer, than the half-space cooling model predicts.

We then examine Curie depth variations with age within the three sub-regions of Euler poles, i.e., area to the north of the Ellice Basin and the CliF, area to the south and southwest of the LTI-EVC, and area in between (Figure 1). Again, very similar patterns are observed, showing undulating but overall increasing Curie depth with age, except for shallowing around 100 to 140 Ma (Figure 7). For lithosphere younger than ~50 Ma, the area to the north of the Ellice Basin and the CliF appears to have Curie depth variations closer to the half-space cooling model than in other areas.

A further comparison between the Pacific and North Atlantic can be made in the gridded heat flow. In both regions, we grid the heat flow with the same 1° interval in both longitude and latitude. From the plots of heat flow versus crustal age (Figure 8), we find that, for crust younger than ~60 Ma, gridded Pacific heat flows are significantly lower than the half-space cooling model, but the model fits gridded North Atlantic heat flow reasonably well (Figure 8). From visual inspection of Figure 8, the turning point of heat flow from being predominantly lower to higher than the theoretical curve occurs earlier in the Pacific, at about 70 Ma, than at about 95 Ma in North Atlantic. These observations may imply stronger hydrothermal circulation in the Pacific than in the North Atlantic, and are in line with the Curie depth contrast near the ridge crest for crust younger than 5 Ma. We speculate that stronger hydrothermal circulation in the Pacific may have persisted from the youngest oceanic lithosphere to lithosphere of ~60 Ma old.

4.2 East Pacific Rise and Other Active Spreading Centers

Even though Curie depths are mostly shallower close to the ridge, the most peculiar pattern is observed for crust younger than ~5 Ma: Curie depths increase toward the ridge axis, instead of decreasing. This phenomenon is clearly seen from the Curie depth variation with age (Figures 6 and 7), and can also be observed from the map view of the Curie depth model by carefully tracing along the 0 Ma isochron (Figure 5). This result is surprising and at odds with previous studies. In the North Atlantic ridge case, we did not observe this deepening of Curie points at the mid-ocean ridge (Li C-F et al., 2013), suggesting that the algorithm works for mid-ocean ridge settings. This is not a resolution artifact because this pattern persists for the entire Pacific ridge and exists within the ~5 Ma isochrons.

We plot Curie depths within the first 15 Ma to better view their increase toward the ridge crest (Figure 9). Since this pattern is present not only on the total Curie depth plot (a), but also on individual plots from different sub-regions (b, c and d), it is unlikely to be a computational artifact; we suggest that it has true geological meaning behind it. Our global survey also shows that fast and superfast spreading centers exhibit Curie points of the largest and intermediate depths, respectively (Li C-F et al., 2017). A decrease in magnetization amplitude with age and high amplitude of axial anomalies has been observed (Klitgord et al., 1975; Johnson and Atwater 1977; Bleil and Peterson, 1983; Guyodo and Valet, 1999; Gee et al., 2000). However, our algorithm is based on wavenumber only, and is totally independent of magnetization amplitude.

The chemical and mineralogical composition near the fast-spreading ridge crest could be so distinct that it would require a different Curie temperature. Superfast spreading might also cause partial melting at a slightly lower temperature. Although it is difficult to quantify these effects, it is unlikely that these effects can be so dramatically revealed by a large Curie depth anomaly near the ridge.

The youngest oceanic crust proximal to the ridge crest is regarded as having the strongest crust-scale hydrothermal circulation (e.g. Hasenclever et al., 2014), because it has the highest thermal gradient and the thinnest lithosphere. Decompressional partial melting and the presence of a magma chamber can further intensify upward percolation of hydrothermal fluids. These processes could preferably cool down the lithosphere near the ridge. By comparison, no such crest Curie depth anomaly was ob-

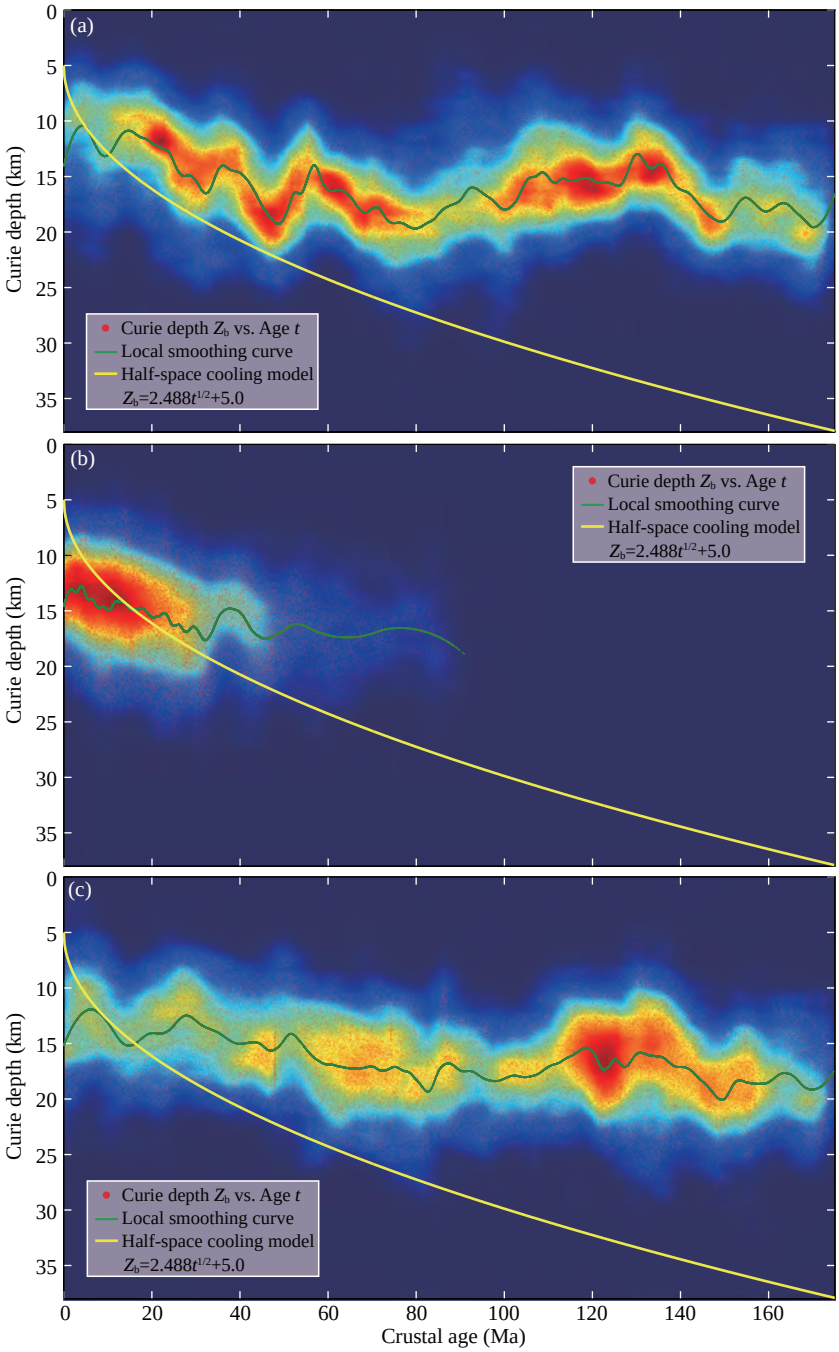

Figure 7. Curie depth (Z_b) variations with crustal ages (t) for three sub-regions of the Pacific. (a) Data from the region to the north of the Line-Tuamotu Islands-Easter Volcanic Chain (LTI-EVC). (b) Data from the region between the CliF and LTI-EVC. (c) Data from the region to the south and southwest of the LTI-EVC. See Figure 6 for more annotations.

served along the slow spreading ridge in North Atlantic (Li C-F et al., 2013). These observations seem conform with early findings that the spreading rate is a major factor controlling ridge melting and hydrothermal circulation (e.g., Chen TJ and Phipps Morgan, 1996). Recent work shows that a proportion of slowly spreading oceanic crust has undergone amagmatic accreation that brings lower crust and upper mantle to the seafloor and becomes serpentinized and magnetized (Tucholke et al., 1998). This may have certain effects on hydrothermal systematics. Certainly, within just a few kilometers of the axis, the Curie depth must lie above the axial melt lens. However, the spatial averaging of our technique, based on spectra from large computational windows, is not likely to resolve the shallow Curie depth within just a few kilometers of the axis.

The scaling (spatial correlation) of magnetization near the fast spreading ridge might be fundamentally different from other parts of the oceanic crust, such that we may have under-corrected it with a smaller β^p_{3D}. From surface magnetic anomalies, and equivalent magnetization (Dyment et al., 2015), we can observe patchy, long-wavelength and large-amplitude magnetic anom-

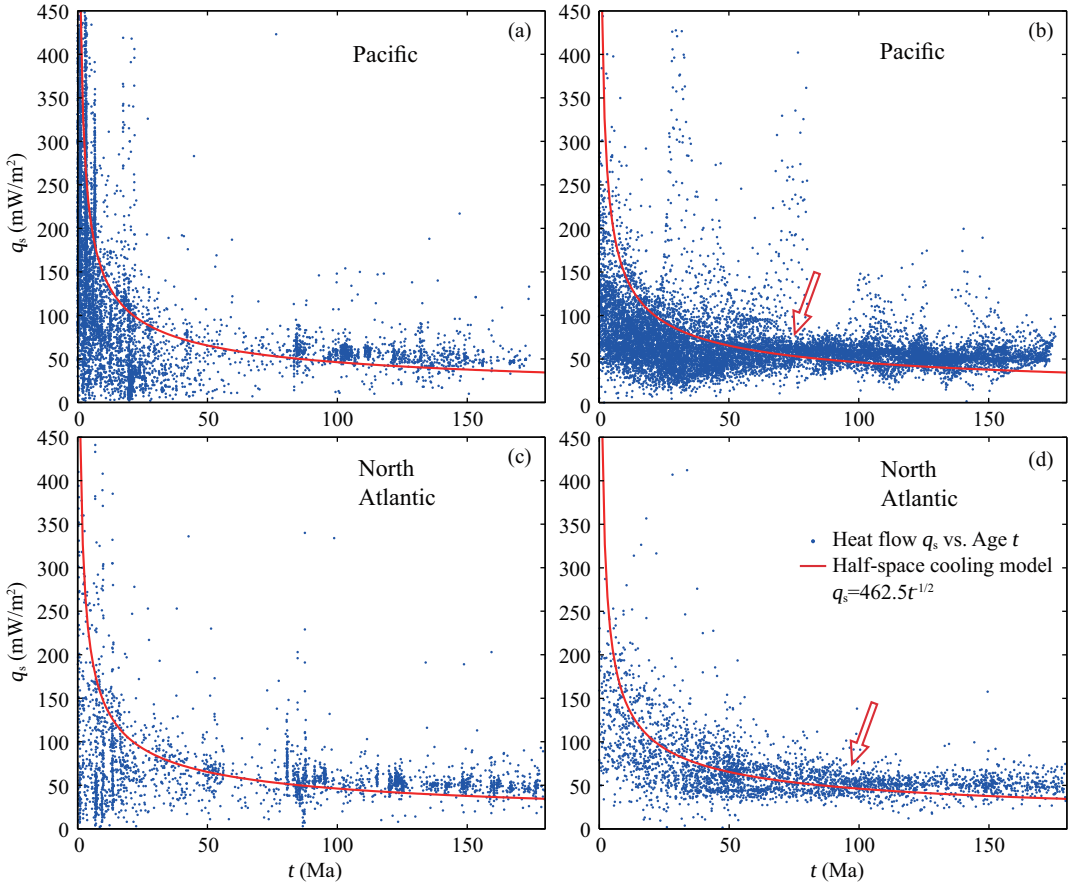

Figure 8. Comparison of heat flow between the Pacific and North Atlantic. The arrow points to the turning point of heat flow from being predominantly lower to higher than that from a half space cooling model. (a) Plot of original heat flow versus crustal ages in the Pacific. (b) Plot of gridded heat flow versus crustal ages in the Pacific. (c) Plot of original heat flow versus crustal ages in the North Atlantic. (d) Plot of gridded heat flow versus crustal ages in the North Atlantic. Red curves show predicted heat flow from the half-space cooling model.

alies near the active spreading centers of the Pacific (Figures 3 and 10); such anomalies are nearly absent in the slow spreading North Atlantic ridge. We believe that it is these long-wavelength anomalies that lead to larger calculated Curie depths near the ridge. They are observed not only along the East Pacific Rise but also along the Juan de Fuca Ridge and the Galapagos spreading center between the Cocos and Nazca plates (Figure 10). These patchy positive and negative magnetic anomalies could be related to magmatic or hydrothermal processes unique to fast and superfast spreading centers. These features along the fast mid-ocean ridge are surely not the results of fast spreading rates, otherwise they should also be present in other parts of the Pacific, not just limited to areas around the ridge. Their true origins need to be better studied.

4.3 Seamounts and Oceanic Plateaus

Our Curie depth model indicates rather complex thermal structures beneath Pacific seamounts and oceanic plateaus. Major known active hot spots (e.g., Clouard and Bonneville, 2001) are all located where the Curie depths are anomalously shallow (Figuers 1 and 5). Furthermore, the seamount trails behind the hot spots also show distinctly shallower Curie depths than their adjacent areas, suggesting the presence of hot lines associated with these hot spots. These characteristics are not observed from the surface heat flow map (Figure 2). No obvious waning or waxing in Curie depth variations is observed along these seamount trails, and this is particularly true for the Emperor-Hawaii seamount chain, which shows notably small Curie depths throughout its entire track (Figure 5). This is mysterious and against our common perception that there could be age-progressive changes in thermal structures of seamount trails if they are from deep mantle plumes of higher temperatures. We suspect that late-stage thermal rejuvenation could have been more focused along these seamount chains, as presumably they are weak zones with deep roots. In fact, most of these seamounts in northwestern Pacific, the oldest part of the Pacific Plate, e.g., the Wake Seamounts (WS), are accompanied with shallow Curie depths, likely caused by pervasive late-stage thermal rejuvenation as well as lithospheric weakening along the seamount chains.

Most of the major Pacific oceanic plateaus do not show notable Curie depth anomalies, except for the Hess Rise. The Tamu Massif in the southwest segment of the Shatsky Rise (SR) and a large part of the Ontong-Java Plateau and Mid-Pacific Mountains show large Curie depths. We speculate that these Mesozoic plateaus have cooled resulting in deep Curie depths, but in places such as near the Hess Rise they may have been thermally rejuvenated to show small Curie depths. Further studies on the deep structures and

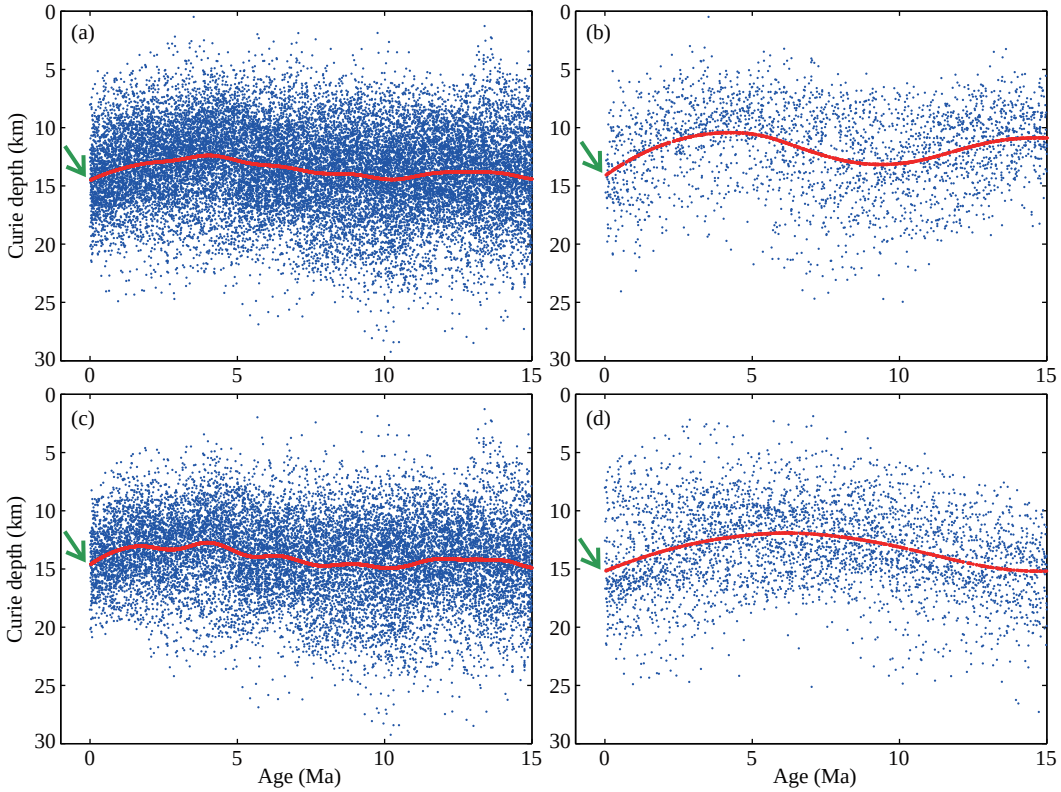

Figure 9. Unusual but consistent increase in Curie depths with decreasing crustal ages towards the ridge crest. The arrows point to the ridge crest. (a) Plot of all Curie depths versus ages. (b) Plot of Curie depths versus ages from the region to the north of the LTI-EVC. (c) Plot of Curie depths versus ages from the region between the CliF and LTI-EVC. (d) Plot of Curie depths versus ages from the region to the south and southwest of the LTI-EVC.

thermal field are needed to better understand the mechanism of thermal rejuvenation.

4.4 Fracture Zones

As mentioned earlier, the large fracture zone associated with the Line-Taumotu Islands-Easter Volcanic Chain shows shallow Curie depths, indicating a thermal anomaly. A few of others, like the Clarion Fracture Zone (ClaF) and Clipperton Fracture Zone (CliF), also have shallow Curie depth anomalies, although not so obvious as those of seamount trails. We also attribute these thermal anomalies to weakening of the lithosphere and possible thermal perturbation along fracture zones.

5. Conclusions

In this paper, we have sought to infer the thermal structure of the Pacific lithosphere from Curie depths estimated from magnetic anomalies. We make the following major conclusions.

(1) Reflecting the cooling of oceanic lithosphere, Pacific Curie depths increase on the first order with crustal age, but undulate frequently, and show an anomalous shallowing for crustal ages between ~100 and ~140 Ma.

(2) Abnormally large Curie depths are found along nearly the entire ridge crest of the East Pacific Rise and other active spreading centers in the Pacific (Juan de Fuca Ridge and the Galapagos Ridge). From about the 5 Ma isochrons, Curie depths increase toward the ridge crest. We find that, near the active spreading centers, uniquely developed patchy, long-wavelength and large-amplitude magnetic anomalies have led to these calculated large Curie depth anomalies. These anomalies are most likely caused by magmatic or hydrothermal processes that prevail near the fast and super-fast spreading centers in the Pacific, but not near the slow spreading centers in the North Atlantic.

(3) All known active hot spots, most seamount trails, and some major fracture zones are accompanied by shallow Curie depths, suggesting that their thermal anomalies are caused either by active magmatism or late-stage thermal rejuvenation. A large zone of shallow Curie depths along the Line-Taumotu Islands -Easter Volcanic Chain and its northwest extension almost bisects the Pacific. Most Mesozoic oceanic plateaus, however, do not show notably anomalous Curie depths.

(4) Curie depth is much more indicative of deep thermal anomalies than surface heat flow, which is more strongly influenced by hydrothermal processes and sediment properties.

(5) There are many large contrasts in the thermal evolution between the Pacific and North Atlantic. A deep Curie depth anomaly is observed near the fast/super-fast spreading Pacific ridge but not along the slow spreading North Atlantic ridge. Both Curie depth and heat flow variations with crustal age support much stronger hydrothermal circulation occurring in Pacific basin lithosphere younger than ~60 Ma. Yet, at the larger lithospheric

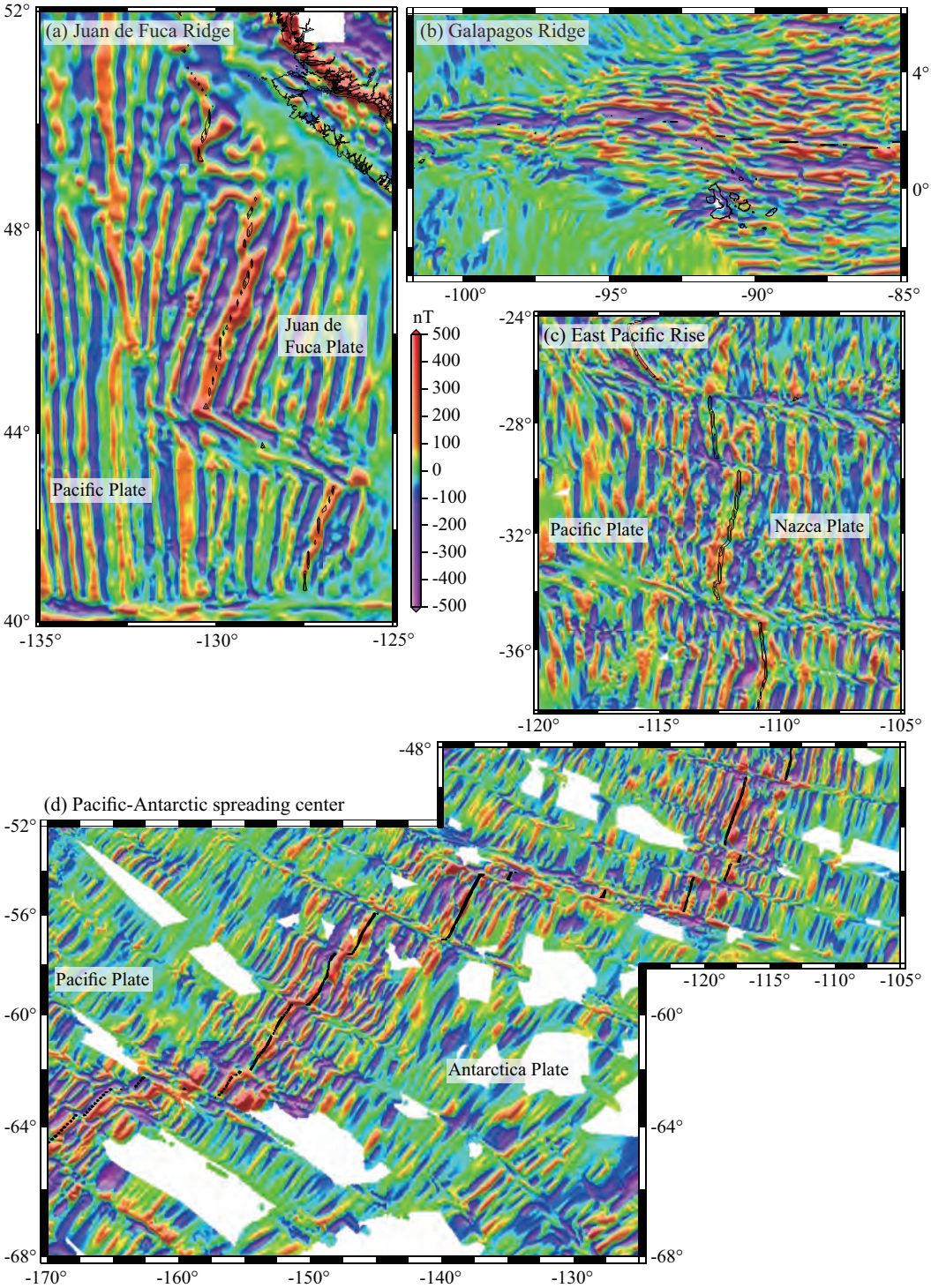

Figure 10. Magnetic anomalies from EMAG2 (Maus et al., 2009) showing patchy, long-wavelength and large-amplitude magnetic anomalies along the active spreading centers at different regions of the Pacific.

depths of Curie depths, our Curie depth model argues for a warmer Pacific lithosphere for crustal ages older than ~15 Ma, given a slightly higher spatial correlation of magnetization in the Pacific than in the North Atlantic.

(6) Our Curie depth model as a function of age suggests that magnetization and serpentinization of the upper mantle from hydrothermal circulation may start to occur very near the fast spreading ridge. Widespread upper mantle serpentinization happens in the entire evolutionary history of the oceanic lithosphere, as seawater percolates through fractures and veins into the upper mantle.

Acknowledgement

This research is funded by the National Natural Science Founda-

tion of China (Grant Nos. 41776057, 41761134051, 41704086 and 91428309). Data processing and mapping is supported by GMT (Wessel and Smith, 1995) and the USGS potential field software (Cordell et al., 1993; Phillips, 1997). The original Earth Magnetic Anomaly Grid of 2-arc-minute resolution (EMAG2) is downloaded from http://geomag.org/, and heat flow data are from the Global Heat Flow Database of the International Heat Flow Commission (http://www.heatflow.und.edu/).

References

Adam, C., and Vidal, V. (2010). Mantle flow drives the subsidence of oceanic plates. *Science*, *328*(5794), 83–85. https://doi.org/10.1126/science.1185906

Arkani-Hamed, J. (1989). Thermoviscous remanent magnetization of oceanic lithosphere inferred from its thermal evolution. *J. Geophys. Res.*, *94*(B12), 17421–17436. https://doi.org/10.1029/JB094iB12p17421

Ballmer M. D., Ito, G., van Hunen, J., and Tackley, P. J. (2010). Small-scale sublithospheric convection reconciles geochemistry and geochronology of 'superplume' volcanism in the western and south Pacific. *Earth Planet. Sci. Lett.*, *290*(1-2), 224–232. https://doi.org/10.1016/j.epsl.2009.12.025

Bansal, A. R., Gabriel, G., Dimri, V. P., and Krawczyk, C. M. (2011). Estimation of depth to the bottom of magnetic sources by a modified centroid method for fractal distribution of sources: An application to aeromagnetic data in Germany. *Geophysics*, *76*(3), L11–L22. https://doi.org/10.1190/1.3560017

Billen, M. I., and Stock, J. (2000). Morphology and origin of the Osbourn Trough. *J. Geophys. Res.*, *105*(B6), 13481–13489. https://doi.org/10.1029/2000JB900035

Blakely, R. J. (1995). *Potential Theory in Gravity and Magnetic Applications*. Cambridge: Cambridge University Press.

Bleil, U., and Peterson, N. (1983). Variations in magnetization intensity and low temperature titanomagnetite oxidation of ocean floor basalts. *Nature*, *301*(5899), 384–388. https://doi.org/10.1038/301384a0

Bonatti, E., and Harrison, C. G. A. (1976). Hot lines in the Earth's mantle. *Nature*, *263*(5576), 402–404. https://doi.org/10.1038/263402a0

Bouligand, C., Glen, J. M. G., and Blakely, R. J. (2009). Mapping Curie temperature depth in the western United States with a fractal model for crustal magnetization. *J. Geophys. Res.*, *114*(B11), B11104. https://doi.org/10.1029/2009JB006494

Carlson R. L., and Johnson, H. P. (1994). On modeling the thermal evolution of the oceanic upper mantle: An assessment of the cooling plate model. *J. Geophys. Res.*, *99*(B2), 3201–3214. https://doi.org/10.1029/93JB02696

Chen, Y. J., and Phipps Morgan, J. (1996). The effects of spreading rate, the magma budget, and the geometry of magma emplacement on the axial heat flux at mid-ocean ridges. *J. Geophys. Res.*, *101*(B5), 11475–11482. https://doi.org/10.1029/96JB00330

Chiozzi, P., Matsushima, J., Okubo, Y., Pasquale, V., and Verdoya, M. (2005). Curie-point depth from spectral analysis of magnetic data in central-southern Europe. *Phys. Earth Planet. Inter.*, *152*(4), 267–276. https://doi.org/10.1016/j.pepi.2005.04.005

Clouard, V., and Bonneville, A. (2001). How many Pacific hotspots are fed by deep-mantle plumes?. *Geology*, *29*(8), 695–698. https://doi.org/10.1130/0091-7613(2001)029<0695:HMPHAF>2.0.CO;2

Collette, B. J. (1974). Thermal contraction joints in a spreading seafloor as origin of fracture zones. *Nature*, *251*(5473), 299–300. https://doi.org/10.1038/251299a0

Cordell, L., Phillips, J. D., and Godson, R. H. (1993). USGS potential-field geophysical software for PC and compatible microcomputers. *Lead. Edge*, *12*(4), 290. https://doi.org/10.1190/1.1436952

Davaille, A. (1999). Simultaneous generation of hotspots and superswells by convection in a heterogeneous planetary mantle. *Nature*, *402*(6763), 756–760. https://doi.org/10.1038/45461

Davies, G. F. (1988). Ocean bathymetry and mantle convection: 2. Small scale flow. *J. Geophys. Res.*, *93*(B9), 10481–10488. https://doi.org/10.1029/JB093iB09p10481

Davis, A. S., Gray, L. B., Clague, D. A., and Hein, J. R. (2002). The Line Islands revisited: New $^{40}Ar/^{39}Ar$ geochronologic evidence for episodes of volcanism due to lithospheric extension. *Geochem. Geophys. Geosyst.*, *3*(3), 1–28. https://doi.org/10.1029/2001GC000190

Downey, N. J., Stock, J. M., Clayton, R. W., and Cande, S. C. (2007). History of the Cretaceous Osbourn spreading center. *J. Geophys. Res.*, *112*(B4), B04102. https://doi.org/10.1029/2006JB004550

Dyment, J., Choi, Y., Hamoudi, M., Lesur, V., and Thebault, E. (2015). Global equivalent magnetization of the oceanic lithosphere. *Earth Planet Sci. Lett.*, *430*, 54–65. https://doi.org/10.1016/j.epsl.2015.08.002

Farrar, E., and Dixon, J. M. (1981). Early Tertiary rupture of the Pacific plate: 1700 km of dextral offset along the Emperor trough-Line Islands lineament. *Earth Planet. Sci. Lett.*, *53*(3), 307–322. https://doi.org/10.1016/0012-821X(81)90036-4

Ferré, E. C., Friedman, S. A., Martín-Hernández, F., Feinberg, J. M., Conder, J. A., and Ionov, D. A. (2013). The magnetism of mantle xenoliths and potential implications for sub-Moho magnetic sources. *Geophys. Res. Lett.*, *40*(1), 105–110. https://doi.org/10.1029/2012GL054100

Forsyth, D. W. (1977). The evolution of the upper mantle beneath mid-ocean ridges. *Tectonophysics*, *38*(1-2), 89–118. https://doi.org/10.1016/0040-1951(77)90202-5

Gee, J., Cande, S. C., Hildebrand, J. A., Donnelly, K., and Parker, R. L. (2000). Geomagnetic intensity variations over the past 780 kyr obtained from near-seafloor magnetic anomalies. *Nature*, *408*(6814), 827–832. https://doi.org/10.1038/35048513

Gomez, O., and Briais, A. (2000). Near-axis seamount distribution and its relationship with the segmentation of the East Pacific Rise and northern Pacific-Antarctic Ridge, 17°N-56°S. *Earth Planet. Sci. Lett.*, *175*(3-4), 233–246. https://doi.org/10.1016/S0012-821X(99)00305-2

Guyodo, Y., and Valet, J. P. (1999). Integration of volcanic and sedimentary records of paleointensity: Constraints imposed by irregular eruption rates. *Geophys. Res. Lett.*, *26*(24), 3669–3672. https://doi.org/10.1029/1999GL008422

Hasenclever, J., Theissen-Krah, S., Rüpke, L. H., Morgan, J. P., Iyer, K., Petersen, S., and Devey, C. W. (2014). Hybrid shallow on-axis and deep off-axis hydrothermal circulation at fast-spreading ridges. *Nature*, *508*(7497), 508–512. https://doi.org/10.1038/nature13174

Hasterok, D. (2013). Global patterns and vigor of ventilated hydrothermal circulation through young seafloor. *Earth Planet. Sci. Lett.*, *380*, 12–20. https://doi.org/10.1016/j.epsl.2013.08.016

Hasterok, D., Chapman, D. S., and Davis, E. E. (2011). Oceanic heat flow: Implications for global heat loss. *Earth Planet. Sci. Lett.*, *311*(3-4), 386–395. https://doi.org/10.1016/j.epsl.2011.09.044

Heydolph, K., Murphy, D. T., Geldmacher, J., Romanova, I. V., Green, A., Hoernle, K., Weiss, D., and Mahoney, J. (2014). Plume versus plate origin for the Shatsky Rise oceanic plateau (NW Pacific): Insights from Nd, Pb and Hf isotopes. *Lithos*, *200-201*, 49–63. https://doi.org/10.1016/j.lithos.2014.03.031

Hilde, T. W. C., Isezaki, N., and Wageman, J. M. (1976). Mesozoic sea-floor spreading in the North Pacific. In G. H. Sutton, et al. (Eds.), *The Geophysics of the Pacific Ocean Basin and Its Margin* (pp. 205–226). Washington, D. C.: American Geophysical Union. https://doi.org/10.1029/GM019p0205

Hillier, J. K. (2007). Pacific seamount volcanism in space and time. *Geophys. J. Int.*, *168*(2), 877–889. https://doi.org/10.1111/j.1365-246X.2006.03250.x

Hillier, J. K., and Watts, A. B. (2005). Relationship between depth and age in the North Pacific Ocean. *J. Geophys. Res.*, *110*(B2). https://doi.org/10.1029/2004JB003406

Hoernle, K., Hauff, F., van den Bogaard, P., Werner, R., Mortimer, N., Geldmacher, J., Garbe-Schönberg, D., and Davy, B. (2010). Age and geochemistry of volcanic rocks from the Hikurangi and Manihiki oceanic plateaus. *Geochim. Cosmochim. Acta*, *74*(24), 7196–7219. https://doi.org/10.1016/j.gca.2010.09.030

Huang, J. H., and Zhong, S. J. (2005). Sublithospheric small-scale convection and its implications for the residual topography at old ocean basins and the plate model. *J. Geophys. Res.*, *110*(B5). https://doi.org/10.1029/2004JB003153

Ito, G., and Clift, P. D. (1998). Subsidence and growth of Pacific Cretaceous

plateaus. *Earth Planet. Sci. Lett.*, *161*(1-4), 84–100. https://doi.org/10.1029/2004JB003153

Johnson, H. P., and Atwater, T. (1977). A magnetic study of basalts from the mid-Atlantic ridge at 37°N. *Bull. Geol. Soc. Amer.*, *88*, 637–647. https://doi.org/10.1130/0016-7606(1977)88<637:MSOBFT>2.0.CO;2

Kerr, A. C., and Mahoney, J. J. (2007). Oceanic plateaus: problematic plumes, potential paradigms. *Chem. Geol.*, *241*(3-4), 332–353. https://doi.org/10.1016/j.chemgeo.2007.01.019

Kim, S.-S., and Wessel, P. (2011). New global seamount census from altimetry-derived gravity data. *Geophys. J. Int.*, *186*(2), 615–631. https://doi.org/10.1111/j.1365-246X.2011.05076.x

King, S., and Ritsema, J. (2000). African hot spot volcanism: small-scale convection in the upper mantle beneath cratons. *Science*, *290*(5494), 1137–1140. https://doi.org/10.1126/science.290.5494.1137

Klitgord, K. D., Heustis, S. P., Mudie, J. D., and Parker, R. L. (1975). An analysis of near-bottom magnetic anomalies: sea-floor spreading and the magnetized layer. *Geophys. J. Int.*, *43*(2), 387–424. https://doi.org/10.1111/j.1365-246X.1975.tb00641.x

Koppers, A. A. P., Morgan, J. P., Morgan, J. W., and Staudigel, H. (2001). Testing the fixed hotspot hypothesis using $^{40}Ar/^{39}Ar$ age progressions along seamount trails. *Earth Planet. Sci. Lett.*, *185*(3-4), 237–252. https://doi.org/10.1016/S0012-821X(00)00387-3

Koppers, A. A. P., Staudigel, H., Pringle, M. S., and Wijbrans, J. R. (2003). Short-lived and discontinuous intraplate volcanism in the South Pacific: Hot spots or extensional volcanism?. *Geochem. Geophys. Geosyst.*, *4*(10), 1089. https://doi.org/10.1029/2003GC000533

Koppers, A. A. P., Staudigel, H., Wijbrans, J. R., and Pringle, M. S. (1998). The Magellan seamount trail: Implications for Cretaceous hotspot volcanism and absolute Pacific Plate motion. *Earth Planet. Sci. Lett.*, *163*(1-4), 53–68. https://doi.org/10.1016/S0012-821X(98)00175-7

Korenaga, T., and Korenaga, J. (2008). Subsidence of normal oceanic lithosphere, apparent thermal expansivity, and seafloor flattening. *Earth Planet. Sci. Lett.*, *268*(1-2), 41–51. https://doi.org/10.1016/j.epsl.2007.12.022

Kruse, S. E., McCarthy, M. C., Brudzinskai, M. R., and Ranieri, M. E. (1996). Evolution and strength of Pacific fracture zones. *J. Geophys. Res.*, *101*(B6), 13731–13740. https://doi.org/10.1029/96JB00645

Li, C.-F. (2011). An integrated geodynamic model of the Nankai subduction zone and neighboring regions from geophysical inversion and modeling. *J. Geodynamics*, *51*(1), 64–80. https://doi.org/10.1016/j.jog.2010.08.003

Li, C.-F., Chen, B., and Zhou, Z. (2009). Deep crustal structures of eastern China and adjacent seas revealed by magnetic data. *Sci. China Ser. D: Earth Sci.*, *52*(7), 984–993. https://doi.org/10.1007/s11430-009-0096-x

Li, C.-F., Lu, Y., and Wang, J. (2017). A global reference model of Curie-point depths based on EMAG2. *Sci. Rep.*, *7*, 45129. https://doi.org/10.1038/srep45129

Li, C.-F., Shi, X. B., Zhou, Z. Y., Li, J. B., Geng, J. H., and Chen, B. (2010). Depths to the magnetic layer bottom in the South China Sea area and their tectonic implications. *Geophys. J. Int.*, *182*(3), 1229–1247. https://doi.org/10.1111/j.1365-246X.2010.04702.x

Li, C.-F., and Wang, J. (2016). Variations in Moho and Curie depths and heat flow in Eastern and Southeastern Asia. *Mar. Geophys. Res.*, *37*(1), 1–20. https://doi.org/10.1007/s11001-016-9265-4

Li, C.-F., Wang, J., Lin, J., and Wang, T. T. (2013). Thermal evolution of the North Atlantic lithosphere: New constraints from magnetic anomaly inversion with a fractal magnetization model. *Geochem. Geophys. Geosyst.*, *14*(12), 5078–5105. https://doi.org/10.1002/2013GC004896

Mahoney, J. J., Duncan, R. A., Tejada, M. L. G., Sager, W. W., and Bralower, T. J. (2005). Jurassic-Cretaceous boundary age and mid-ocean-ridge-type mantle source for Shatsky Rise. *Geology*, *33*(3), 185–188. https://doi.org/10.1130/G21378.1

Mareschal, J. C., and Jaupart, C. (2004). Variations of surface heat flow and lithospheric thermal structure beneath the North American craton. *Earth Planet. Sci. Lett.*, *223*(1-2), 65–77. https://doi.org/10.1016/j.epsl.2004.04.002

Maus, S., Barckhausen, U., Berkenbosch, H., Bournas, N., Brozena, J., Childers, V., Dostaler, F., Fairhead, J. D., Finn, C., … Caratori Tontini F. (2009). EMAG2: A 2-arc-minute resolution Earth Magnetic Anomaly Grid compiled from satellite, airborne and marine magnetic measurements. *Geochem. Geophys. Geosyst.*, *10*(8), Q08005. https://doi.org/10.1029/2009GC002471

Maus, S., Gordan, D., and Fairhead, D. (1997). Curie-temperature depth estimation using a self-similar magnetization model. *Geophys. J. Int.*, *129*(1), 163–168. https://doi.org/10.1111/j.1365-246X.1997.tb00945.x

Maus, S., Sazonova, T., Hemant, K., Fairhead, J. D., and Ravat, D. (2007). National geophysical data center candidate for the world digital magnetic anomaly map. *Geochem. Geophys. Geosyst.*, *8*(6), Q06017. https://doi.org/10.1029/2007GC001643

McNutt, M. K. (2002). Heat flow variations over the Hawaiian Swell controlled by near-surface processes, not plume properties. In E. Takahashi, et al. (Eds.), *Hawaiian Volcanoes: Deep Underwater Perspectives* (pp. 355–364). Washington, D.C.: American Geophysical Union. https://doi.org/10.1029/GM128p0365

McNutt, M. K., and Fischer, K. M. (1987). The south Pacific superswell. In B. Keating, et al. (Eds.), *Seamounts, Islands, and Atolls* (pp. 25–34). Washington, D.C.: American Geophysical Union. https://doi.org/10.1029/GM043p0025

Morgan, W. J. (1972). Deep mantle convection plumes and plate motions. *AAPG Bull.*, *56*(2), 203–213. https://doi.org/10.1306/819A3E50-16C5-11D7-8645000102C1865D

Müller, R. D., Sdrolias, M., Gaina, C., and Roest W. R. (2008). Age, spreading rates, and spreading asymmetry of the world's ocean crust. *Geochem. Geophys. Geosyst.*, *9*(4), Q04006. https://doi.org/10.1029/2007GC001743

Nakanishi, M., Tamaki, K., and Kobayashi, K. (1989). Mesozoic magnetic anomaly lineations and seafloor spreading history of the northwestern Pacific. *J. Geophys. Res.*, *94*(B11), 15437–15462. https://doi.org/10.1029/JB094iB11p15437

O'Connor, J. M., Stoffers, P., and McWilliams, M. O. (1995). Time-space mapping of Easter Chain volcanism. *Earth Planet. Sci. Lett.*, *136*(3-4), 197–212. https://doi.org/10.1016/0012-821X(95)00176-D

Orwig, T. L., and Kroenke, L. W. (1980). Tectonics of the eastern central Pacific basin. *Mar. Geol.*, *34*(1-2), 29–43. https://doi.org/10.1016/0025-3227(80)90139-5

Oufi, O., Cannat, M., and Horen, H. (2002). Magnetic properties of variably serpentinized abyssal peridotites. *J. Geophys. Res.*, *107*(B5), EPM3-1–EPM3-19. https://doi.org/10.1029/2001JB000549

Parsons, B., and McKenzie, D. (1978). Mantle convection and the thermal structure of the plates. *J. Geophys. Res.*, *83*(B9), 4485–4496. https://doi.org/10.1029/JB083iB09p04485

Phillips, J. D. (1997). *Potential-Field Geophysical Software for the PC, version 2.2*. U. S. Geological Survey, Open-File Report, 97–725.

Phipps Morgan, J., and Smith, W. H. F. (1992). Flattening of the sea-floor depth-age curve as a response to asthenospheric flow. *Nature*, *359*(6395), 524–527. https://doi.org/10.1038/359524a0

Ravat, D., Pignatelli, A., Nicolosi, I., and Chiappini, M. (2007). A study of spectral methods of estimating the depth to the bottom of magnetic sources from near-surface magnetic anomaly data. *Geophys. J. Int.*, *169*(2), 421–434. https://doi.org/10.1111/j.1365-246X.2007.03305.x

Ray, J. S., Mahoney, J. J., Duncan, R. A., Ray, J., Wessel, P., and Naar, D. F. (2012). Chronology and geochemistry of lavas from the nazca ridge and easter seamount chain: an ~30 myr hotspot record. *J. Petrol.*, *53*(7), 1417–1448. https://doi.org/10.1093/petrology/egs021

Ritzwoller, M. H., Shapiro, N. M., and Zhong, S. J. (2004). Cooling history of the Pacific lithosphere. *Earth Planet. Sci. Lett.*, *226*(1-2), 69–84. https://doi.org/10.1016/j.epsl.2004.07.032

Sager, W. W. (1992). Seamount age estimates from paleomagnetism and their implications for the history of volcanism on the pacific plate. In: B. H. Keating, et al. (Eds.), *Geology and Offshore Mineral Resources of the Central Pacific Basin* (vol. 14, pp. 21–37). New York, NY: Springer. https://doi.org/10.1007/978-1-4612-2896-7_3

Sandwell, D. T., and Fialko, Y. (2004). Warping and cracking of the Pacific Plate by thermal contraction. *J. Geophys Res.*, *109*(B10), B10411. https://doi.org/10.1029/2004JB003091

Sandwell, D. T., Winterer, E. L., Mammerickx, J., Duncan, R. A., Lynch, M. A., Levitt, D. A., and Johnson C. L. (1995). Evidence for diffuse extension of the Pacific plate from Pukapuka ridges and cross-grain gravity lineations. *J.*

Geophys. Res., *100*(B8), 15087–15099. https://doi.org/10.1029/95JB00156

Schroeder, W. (1984). The empirical age-depth relation and depth anomalies in the Pacific Ocean basin. *J. Geophys. Res.*, *89*(B12), 9873–9883. https://doi.org/10.1029/JB089iB12p09873

Schubert, G., Froidevaux, C., and Yuen, D. A. (1976). Oceanic lithosphere and asthenosphere: thermal and mechanical structure. *J. Geophys. Res.*, *81*(20), 3525–3540. https://doi.org/10.1029/JB081i020p03525

Sharp, W. D., and Clague, D. A. (2006). 50-Ma initiation of Hawaiian-Emperor bend records major change in Pacific Plate motion. *Science*, *313*(5791), 1281–1284. https://doi.org/10.1126/science.1128489

Smith, W. H. F., and Sandwell, D. T. (1997). Global sea floor topography from satellite altimetry and ship depth soundings. *Science*, *277*(5334), 1956–1962. https://doi.org/10.1126/science.277.5334.1956

Smoot, N. C., and King, R. E. (1997). The Darwin Rise demise: the western Pacific guyot heights trace the trans-Pacific Mendocino fracture zone. *Geomorphology*, *18*(3-4), 223–235. https://doi.org/10.1016/S0169-555X(96)00032-3

Stein C. A., and Stein, S. (1992). A model for the global variation in oceanic depth and heat flow with lithospheric age. *Nature*, *359*(6391), 123–129. https://doi.org/10.1038/359123a0

Stein, C., and Stein, S. (2003). Mantle plumes: heat flow near Iceland. *Astron. Geophys.*, *44*(1), 1.8–1.10. https://doi.org/10.1046/j.1468-4004.2003.44108.x

Stein, C. A., and Abbott, D. H. (1991). Heat flow constraints on the South Pacific superswell. *J. Geophys. Res.*, *96*(B10), 16083–16100. https://doi.org/10.1029/91JB00774

Stein, C. A., and von Herzen, R. P. (2007). Potential effects of hydrothermal circulation and magmatism on heatflow at hotspot swells. In G. R. Foulger, et al. (Eds.), *Plates, Plumes and Planetary Processes* (pp. 261–274). USA: Geological Society of America Special Papers.

Stepashko, A. A. (2006). The cretaceous dynamics of the pacific plate and stages of magmatic activity in northeastern Asia. *Geotectonics*, *40*(3), 225–235. https://doi.org/10.1134/S001685210603006X

Tanaka, A., Okubo, Y., and Matsubayashi, O. (1999). Curie point depth based on spectrum analysis of the magnetic anomaly data in East and Southeast Asia. *Tectonophysics*, *306*(3-4), 461–470. https://doi.org/10.1016/S0040-1951(99)00072-4

Tarduno, J. A., Sliter, W. V., Kroenke, L. W., Leckie, M., Mahoney, J. J., Musgrave, R., Storey, M., and Winterer, E. L. (1991). Rapid formation of Ontong Java Plateau by Aptian mantle plume volcanism. *Science*, *254*(5030), 399–403. https://doi.org/10.1126/science.254.5030.399

Taylor, B. (2006). The single largest oceanic plateau: Ontong Java-Manihiki-Hikurangi. *Earth Planet. Sci. Lett.*, *241*(3-4), 372–380. https://doi.org/10.1016/j.epsl.2005.11.049

Timm, C., Hoernle, K., Werner, R., Hauff, F., van den Bogaard, P., Michael, P., Coffin, M. F., and Koppers, A. (2011). Age and geochemistry of the oceanic Manihiki Plateau, SW Pacific: new evidence for a plume origin. *Earth Planet. Sci. Lett.*, *304*(1-2), 135–146. https://doi.org/10.1016/j.epsl.2011.01.025

Tominaga, M., Sager, W. W., Tivey, M. A., and Lee, S.-M. (2008). Deep-tow magnetic anomaly study of the Pacific Jurassic Quiet Zone and implications for the geomagnetic polarity reversal timescale and geomagnetic field behavior. *J. Geophys. Res.*, *113*(B7), B07110. https://doi.org/10.1029/2007JB005527

Tucholke, B. E., Lin, J., and Kleinrock, M. C. (1998). Megamullions and mullion structure defining oceanic metamorphic core complexes on the Mid-Atlantic Ridge. *J. Geophys. Res.*, *103*(B5), 9857–9866. https://doi.org/10.1029/98JB00167

Turcotte, D. L. (1974). Are transform faults thermal contraction cracks?. *J. Geophys. Res.*, *79*(17), 2573–2577. https://doi.org/10.1029/JB079i017p02573

Vallier, T. L., Rea, D. K., Dean, W. E., Thiede, J., Adelseck, C. G. (1981). The geology of Hess Rise, central north Pacific Ocean. In J. Thiede, et al. (Eds.), *Init. Repts. DSDP, 62* (pp. 1031–1072). Washington, D.C.: U. S. Govt. Printing Office.

von Herzen, R. P., Cordery, M. J., Detrick, R., and Fang, C. L. (1989). Heat flow and the thermal origin of hot spot swells: the Hawaiian swell revisited. *J. Geophys. Res.*, *94*(B10), 13 783–13 799. https://doi.org/10.1029/JB094iB10p13783

Wessel, P., and Smith, W. H. F. (1995). New version of the generic mapping tools. *EOS*, *76*(33), 329. https://doi.org/10.1029/95EO00198

Windom, K. E., Seifert, K. E., and Vallier, T. L. (1981). Igneous evolution of Hess rise: Petrologic evidence from DSDP Leg 62. *J. Geophys. Res.*, *86*(B7), 6311–6322. https://doi.org/10.1029/JB086iB07p06311